Paper No. 37

RESPONSE OF CANDIDATE METALLIC SPACE SHUTTLE MATERIALS TO SIMULATED REENTRY ENVIRONMENTS

I. M. Grinberg, E. S. Bartlett, R. G. Luce, *Battelle-Columbus Laboratories, Columbus, Ohio*

ABSTRACT

Coated columbium alloys were evaluated in an experimental program to determine their degradation and reuse capability for the thermal protection system of the space shuttle. Intentionally defected specimens were thermally cycled in either an arc-heated wind tunnel or static furnace environment. The relative effect of the environmental exposures on defect growth, mechanical properties, and surface emittance degradation was determined. Techniques used to characterize the arc-heated wind tunnel environment and to determine the thermal response of the specimens during the exposures are described.

INTRODUCTION

During the early stages of the space shuttle program, coated columbium alloys were investigated as to their ability to provide reradiative thermal protection for those portions of the shuttle vehicle which would attain maximum temperatures of approximately 1590 K during reentry. Of concern in this regard was the effect of coating defects on the system's oxidation resistance and mechanical performance, considering the requirement of 100 flight and reentry missions. Also of interest was the possible surface degradation that could occur due to the reuse missions which could require significant refurbishment of the oxidation-protective, high-emittance coating.

A program was undertaken for NASA Marshall Space Flight Center to develop data on the degradation and reuse capability of coated columbium alloy systems for the space shuttle and to establish defect tolerances, failure modes, and methods of assurance of the integrity of these material systems. Both dynamic, hypersonic shear, reduced-air-pressure, and static, reduced-air-pressure furnace environments were used to expose the materials to simulated reentry thermal profiles. This provided for a comparison of the relative degradation of the specimens resulting from the dynamic and static environments. Detailed flaw growth and mechanical property effects studies were conducted, the results of which are summarized herein. Details of hyperthermal arc-heated wind-tunnel experiments are also presented, with

particular attention given to the techniques used to characterize the environment and measure the specimen surface temperature response during the wind-tunnel exposures.

APPARATUS

Arc-Heated Wind Tunnel Facility

The arc-heated wind-tunnel exposures were conducted in the Battelle-Columbus Aerothermal Research Facility. The facility consists of two separate wind-tunnel legs each of which includes a continuous-flow arc heater, a conical convergent-divergent nozzle, a free-jet test cabin, and a conical convergent-divergent diffuser. The arc-heated gas from either leg exhausts into a common heat exchanger and then to the pressure recovery system which consists of a five-stage steam ejector system. Electrical power for both legs is supplied by a 1.5 mw rectifier substation controlled by a saturable reactor. A schematic layout of the facility is shown in Figure 1.

For these exposures, the nontoxic leg was used with the high-enthalpy arc heater. This arc heater is of a modular design with a segmented column, gas stabilization of the arc column, and separate injection of oxygen and nitrogen. The conical nozzle used has a 2.54 cm diameter throat and a 12.7 cm exit diameter. Test-cabin pressure was maintained at a desired level, consistent with the 12.7 cm exit diameter nozzle and the heater stagnation pressure, by varying the amount of secondary air that was bled into the cabin.

Specimens

The test specimens used for the exposures were nominally 7.6 x 1.9 x 0.05 cm in length, width, and thickness, respectively, with additional length provided for two tabs at each end. The tabs were bent at a nominal radius of 0.05 cm. This configuration permitted mounting of the specimens in the model holder by the insertion of pins into supporting blocks through small holes in the end tabs on the specimens. Six specimens were exposed simultaneously by mounting three specimens on each of two silicide-coated molybdenum blocks which were positioned and held in the water-cooled model holder. Figure 2 shows the molybdenum blocks in the model holder. The pins on the leading edge of the front and rear blocks can be seen in Figure 2. The majority of the block material was machined out in order to reduce the heat conduction losses to the supporting water-cooled structure. Fibrous zirconia thermal insulation was placed in the wells to further reduce heat losses from the specimens.

In order to obtain approximately the same heat flux level on the front and rear specimens, the orientation of the front and rear block relative to the model holder surface could be adjusted

during the exposure. In practice, the angle of attack of the rear block and specimens was set slightly higher than the front block to account for the flat plate heat flux decay with distance from the leading edge. Although the surface discontinuity between front and rear specimens gave rise to a shock wave at their intersection, it was found that the conditions for a major portion of the rear specimens were approximately the same as those for the front specimens. The slight difference in the local Mach numbers between the front and rear specimens is unimportant in terms of material performance.

Model Holder

The specimens and blocks were mounted in a water-cooled model holder 1.9 cm thick, through which passages were machined for water cooling. A photograph of the model holder is shown in Figure 2. The major components of the model holder consist of a flat plate with a 0.31 cm nose radius, an instrumentation block for mounting of the spring-loaded thermocouples, and a housing to shield the instrumentation. Overall dimensions of the model holder are 26 cm long (air-flow direction) and 13.9 cm wide. A cutout having nominal dimensions of 15.7 cm long and 5.9 cm wide was provided in the holder for the specimens and block. The cutout was centered with respect to the width of the holder and extended from 8.9 cm (14 nose diameters) to 24.7 cm from the leading edge of the holder. This location relative to the leading edge was selected in order to reduce pressure and heat flux gradients to a minimum consistent with specimen and nozzle size. The angle of attack of the water-cooled holder was set at approximately 18 degrees with respect to the arc-heated air flow direction.

Instrumentation

Thermocouples, infrared pyrometry, infrared photography, and time-lapse panchromatic photography were used to determine the response of the specimens during plasma arc exposures. Accurate determination of the specimen temperatures was necessary for correlation of the mechanical property data with exposure and for comparison of the effects of the dynamic and static environments on oxidation and mechanical property measurements. A spring-loaded, Pt/Pt-10 Rh thermocouple was used to determine the back-face temperature of each coated columbium specimen during exposure. Thermocouples protruding through holes in the bottom of each support block can be seen in Figure 2. Two infrared-radiation (IR) pyrometers were used during the wind-tunnel exposures to measure the surface temperature of the specimens. The pyrometers are manufactured by Ircon, Inc., and operate in the spectral range of 2.0 to 2.6 μm. Infrared photographs were taken during the nominal peak-temperature-exposure portion of the cyclic exposures to determine the temperature gradients over the entire surface area of the specimens. Black-and-white infrared

522-137 O - 73 - 33

film was used with an 87 C filter over the camera lens. This combination of film and filter limits the radiation detection to a relatively narrow wavelength interval, 0.85 to 0.90 μm. An electrically driven, remote-controlled, Hasselblad camera (70 mm) and a 35 mm Cannon camera were used to obtain these photographs. Time-lapse photographs of the specimens were taken during the exposures to determine the rate of defect growth. A remote-controlled Hasselblad camera was used for these pictures.

Facility instrumentation was also provided to characterize the arc-heater performance. This included arc-heater stagnation pressure, voltage, current, coolant water-flow rate and temperature rise, and gas mass-flow rate. Also, the specimen surface/environmental conditions were measured using instrumented, water-cooled blocks that fit into the water-cooled model holder. These blocks had provisions for surface pressure taps and water-cooled heat flux calorimeters.

The specimen temperatures and arc-heater operating conditions were recorded on the facility's digital data-acquisition system. Since the exposure times per cycle were on the order of one-half hour, data reduction and permanent recordings were made on-line. A complete set of data was printed on the TTY about every 20 seconds. Also, continuous monitoring of the arc-heater conditions and selective data were provided visually on a CRT display.

EXPERIMENTAL PROCEDURES

Columbium Alloy Materials

Three coated columbium alloys were evaluated in thin-sheet form. Substrates were the commercial columbium alloys Cb752 (Cb-10W-2.5Zr), C129Y (Cb-10W-10Hf-0.01Y), and FS85 (Cb-27Ta-10W-0.8Zr). Both Cb752 and FS85 were coated with 80 μm of the commercial oxidation-protective silicide coating R512E (Si-20Cr-20Fe, slurry-fusion process), and C129Y was coated with 80 μm commercial VH109, also a fused slurry silicide. All specimen surfaces were coated. For the application of coated columbium alloys to space shuttle TPS, knowledge of environmental effects upon structural performance is critical. Furthermore, a low, but significant frequency of occurrence of defects in the protective coatings is expected. The response of properties to oxidation/contamination effects at the sites of coating defects represents the "worst case" analysis for coated columbium alloys. For this reason, most specimens were treated to introduce intentional defects by electrical-discharge machining holes (0.1 and 1 mm in diameter) through the coatings. These penetrated about 20 μm into the columbium alloy substrate to insure total coating penetration.

Evaluation of Defect Growth

The rate of growth of defects provides one measure of degradation of structural properties. Substrate metal that is lost through oxidation can no longer support structural loads. Also, for columbium alloys, diffusion of oxygen into the metal matrix embrittles some of the metal surrounding the defect such that it loses some of its load-bearing capability.

Visible defect growth was measured in several ways. Time-lapse photographs taken during aerothermal exposures provided a direct measure of defect growth for many specimens. Radiographs of exposed specimens were inspected to determine the amount that selective substrate oxidation affected undercutting of the coating. Defect growth rates determined by time-lapse photography and before-and-after measurements were adjusted for undercutting on a pro rata basis. In addition, metallographic sections were prepared through the centers of defect sites. From these, metal surface recession (equivalent to 1/2 the defect growth) and depth of hardening of substrate material surrounding the defect via oxygen influx (an indicator of depth of embrittlement) were measured. Measurements were converted to the appropriate rates by factoring according to total time at the maximum exposure temperature for each intentional coating defect site.

Specimen Thermal Characterization

Spring-loaded, 28-gauge, backface thermocouples were used to obtain a continuous record of temperature for one location per specimen. To avoid reactions of the thermocouple material with the specimen's disilicide coating, a 25 μm-thick, 0.3-cm square, platinum foil was attached to the coated columbium using a thin application of Sauereisen No. 8 Electrotemp refractory cement. This was found experimentally to be reasonably compatible with both R512E and VH109 coatings under nominal thermal conditions. The spring-loaded device forced contact of the thermocouple bead against the platinum foil cemented to the underside of the specimen. Chemical compatibility experiments were conducted to determine possible effects of the cement and foil on the thermocouple output at elevated temperature. No deleterious effects were obtained.

Two infrared pyrometers were used during the arc-heated wind-tunnel exposures. One of the pyrometers (control pyrometer) was fixed and sighted on the middle specimen in the front row, approximately in the center of the specimen, and was used for control of the arc heater during the heatup and cooldown portions of the cycles. The second pyrometer (scanning pyrometer) was used to obtain data on the surface temperature profile of the specimens. This pyrometer was mounted on a remote-controlled traversing mechanism which permitted the pyrometer to scan over the specimens during the exposures. In this manner, it was

possible to obtain one or more complete scans in the side-to-side and flow directions. The voltage output of a positioning potentiometer (which indicated the precise pyrometer scan location) was recorded simultaneously with the pyrometer output voltage. The pyrometer scan speed was adjusted to a maximum compatible with the response characteristics of the pyrometer. The pyrometer temperature-voltage calibration tabulations were experimentally corrected for arc radiation reflected from the specimen surface at operating conditions identical to those used during the specimen exposures. Also, because the pyrometers were mounted on top of the test cabin, it was necessary to correct the signals for radiation attenuation due to the test cabin window. This was accomplished experimentally by measuring the change obtained in pyrometer signal with and without the window as a function of source temperature.

Infrared photography was used to obtain periodic total specimen area records of the surface temperature distribution. Several exposure durations and f-stops were used depending on the specimen surface temperature. The cameras were mounted on top of the test cabin and were sighted on the specimens through the test-cabin window. Calibration of the infrared film was accomplished using a technique similar to that described by Pollack and Hickel.[1] In this calibration, the density of the film is uniquely related to the source or specimen brightness temperature. In essence, the procedure consists of three key elements: (1) a calculated relationship between the surface temperature and the relative radiant energy, which results in a master distribution curve (MTD curve); (2) an experimentally determined relationship between film density and the relative film exposure energy, which results in a film response curve (FR curve); and (3) a calibration point which is a known temperature on the specimen surface that can be associated with a corresponding film density. The first two elements are independently determined and are associated with each other by the temperature-density calibration point. Calibrations were performed for both the 70 mm and 35 mm infrared films. Details of the calibration procedures can be found in References (2) and (3).

A representative black-and-white infrared photograph obtained during the arc-heated wind-tunnel exposures is shown in the bottom photograph of Figure 3. Light regions represent hotter areas, and dark regions are indicative of cooler areas. Contours of the specimen surface temperature were generated using infrared positive transparencies and the temperature-film density calibration. This detailed contour mapping was useful in that specimen temperatures at the various defect sites could be obtained simultaneously with considerable accuracy. Specimen surface temperature contours were also obtained by color-enhancing the black-and-white infrared photograph. A color-enhanced (black-and-white in the publication) picture of the black-and-white infrared photograph in Figure 3 (bottom) is shown as the

top photograph in Figure 3. Each color represents a photographic density interval considered to be a region of constant temperature (in the publication, these colors appear as various shades of gray). The temperature range represented by each of the eight colors in Figure 3 is approximately 20 K. A finer increment in temperature can be achieved by selecting a finer density interval on the Data-Color System. This would result in a greater number of constant density intervals for the density range of the photograph.

During the arc-heated wind-tunnel exposures, apparent emittance variations were noted from cycle to cycle on multicycle runs by comparing the output of the control pyrometer with the temperature obtained from the backface thermocouple as cycling progressed. Apparent emittance changes were also observed by considering the arc heater power level (enthalpy) required to maintain a fixed nominal specimen temperature from cycle to cycle.

Environment Thermal Characterization

The arc-heated air environment was characterized to define free-stream and local surface conditions. Characterizations were obtained for the arc-heater operating conditions used during the exposures of the columbium alloy specimens. A summary of the environment characterization data is given in Tables 1 and 2.

The free-stream Mach number was calculated for the 12.7 cm exit diameter nozzle using a chemically reacting nozzle flow program based on the analytic technique developed by Lordi, et al[4], for nonequilibrium expansions of reacting gas mixtures. Also, a laminar boundary layer program based on the Cohen and Reshotko[5] solution with heat transfer and arbitrary pressure gradient was used. The arc-heater reservoir pressure was measured experimentally using a pressure transducer and the gas total enthalpy was determined using the energy balance technique.

Surface shear stresses were calculated using a technique described by Harney and Petrie[6]. In this procedure, the flowfield equations are formulated in a manner that brings out their explicit dependence on gas thermodynamic and transport properties with minimal dependence on Mach number. The skin-friction coefficient is expressed in terms of surface and free-stream flow properties. Numerical values for the free-stream flow properties were obtained from the solution of the nonequilibrium nozzle flow expansion. Surface pressures and heat-transfer rates were measured experimentally using water-cooled copper blocks which fit into the spaces occupied by the specimens and molybdenum blocks that were used during the material exposures. Both front and rear calorimeter blocks had three pressure taps and two heat flux calorimeters to determine the axial pressure and heat-transfer rate distributions. An average pressure representative of the

front and rear water-cooled blocks were within 0.01 kN/m^2 of each other, with variations of less than $\pm$ 0.37 kN/m^2 on the front and rear blocks.

A summary of the measured heat-transfer rates for the two nominal operating conditions is shown in Table 2 along with heat-transfer rates calculated using two separate correlation techniques. It can be seen that there is good agreement between the measured and calculated heat-transfer rates.

The nominal simulated time-temperature reentry profiling condition used in dynamically cycling the columbium alloy specimens is as follows:

(1) Heat specimens to 1061 K in approximately 2 minutes

(2) Hold at 1061 K for 5 minutes

(3) Heat to 1561 K or 1644 K, depending on nominal temperature level desired, in approximately 2 minutes

(4) Hold at nominal temperature level 1561 K or 1644 K for 15 minutes

(5) Cool to approximately 977 K in approximately 6 minutes

(6) Repeat (1) through (5) for desired number of exposure cycles.

EXPERIMENTAL RESULTS

Temperature Determination

A typical comparison of all three methods used for determining the specimen surface temperatures (thermocouples, infrared pyrometry, and infrared photography) is shown in Figure 4 for a representative exposure. In this figure, the specimen surface temperature is plotted as a function of distance across the specimens. Also shown are the temperatures indicated by two of the spring-loaded thermocouples. It can be seen that there is good agreement among the temperature-measuring techniques with a maximum difference of approximately 22 K occurring between temperatures obtained from the pyrometer and photographic techniques. This maximum difference is representative of those obtained from similar comparisons of other arc-heated wind-tunnel runs.

Specimen Surface Emittance

The general appearance of the coated columbium alloy specimens was different for the static furnace and arc-heated wind-tunnel exposures. Specimens exposed to the furnace environment developed oxides, the colors of which depended primarily on the coating, and to a lesser extent, upon the substrate. For example, specimens coated with VH109 developed a greenish-brown color,

R512E/Cb752 specimens oxidized to an orange-brown color, and R512E/FS85 oxidized to a reddish-brown color. In contrast, these coating/substrate combinations exhibited fine-textured, cream-colored or white oxide coatings when exposed to the arc-heated wind-tunnel environment.

Apparent emittance variations noted from cycle to cycle on the basis of the arc-heater power level required to maintain the nominal specimen temperature are shown in Figure 5 (circular symbols). It can be seen that there is a relatively large decrease in apparent emittance from the first to the third exposure cycle, with relatively little change occurring in subsequent cycles. Also shown in Figure 5 are apparent emittance changes obtained by comparing the output of the control pyrometer with the temperature indicated by the corresponding backface thermocouple (square symbols). Although this correlation does not yield as rapid an apparent decrease in emittance within the first three cycles, the trend of the data is quite similar and toward decreasing emittance with increasing number of exposures cycles. Both correlation techniques indicate similar emittance values after 8 to 10 exposure cycles.

Apparent changes in specimen emittance can also be illustrated by considering the pyrometer output signal and the indicated thermocouple temperature during the cooldown portion of the cycle. The changes in emittance for the 10-cycle run are shown in Figure 6. The symbols represent the pyrometer output signal and thermocouple temperature at corresponding times. Lines of constant emittance are also shown. It can be seen that there is an apparent decrease in specimen emissivity during the multicycle exposures. The decrease is roughly the same as is obtained by considering the nominal maximum-temperature portion of the cycles as was illustrated in Figure 5. Pyrometer output-temperature data are not shown for the fourth cycle since this cycle was terminated early during the cooldown (specimen temperature of approximately 1476 K).

In contrast with these apparent emittance changes resulting from the arc-heated wind-tunnel exposures, there was little, if any, change in specimen surface emittance noted for those specimens exposed in the furnace environments.

Defect Growth

The maximum intended temperature for the initial exposure series of arc-heated wind-tunnel exposures was 1644 K. Under these high-mass-flow conditions, unexpectedly rapid growth of several intentional coating defects was observed in only one simulated reentry cycle. Figure 7 shows the appearance of a group of six specimens following a 15-minute exposure at 1644 K, nominal. The unlettered specimen is included to illustrate specimen appearance before exposure for comparison. Each

specimen contained one 0.1-mm defect (barely visible in its orientation at the left of the "before" specimen) located forward relative to the flow, and two 1-mm defects, located "center" and "aft". Several of the individual defects in the figure show obvious growth. Also apparent is "wash" from oxidation product effluent swept from the defects by the hypersonic flow. Analysis of temperatures at individual defect sites for several such exposure runs allowed correlations between local exposure temperature and defect growth rates as shown in Figure 8. Neither defect type, location, nor coating type influenced the onset of rapid growth independently from temperature. Substrate composition, however, did have some influence. At exposure temperatures less than about 1620 K, defect growth resulting from the oxidation of any of the columbium alloy substrates was well controlled, and occurred at a rate on the order of 1 μm/min. As the exposure temperature at defect sites exceeded about 1625 K, defect growth rates increased precipitously for the C129Y and Cb752 alloy substrates, and rates as great as 0.5 mm/min of exposure were observed. The FS85 alloy substrate was not nearly so sensitive to aerothermal degradation, as rapid defect growth was not observed even at temperatures as great as 1690 K.

Ambient-pressure furnace oxidation tests of coated-plus-defected Cb752 and C129Y showed that a temperature of at least 1705 K was needed to initiate similar rapid-defect-growth under static conditions. This is about 80 K greater than the threshold temperature under hypersonic shear conditions.

Rapid defect growth under either static or dynamic conditions is associated with melting of columbium oxide. The resulting catastrophic oxidation occurs so rapidly that embrittlement of the remaining metal by solid-state oxygen diffusion is not of much consequence. Figure 9 shows a defect which had grown from an initial size of 0.01 cm to about 0.33 cm in one wind-tunnel exposure cycle. By comparison, the visible contamination front has advanced to a depth of only about 0.01 cm from the oxide-metal interface.

During arc-heated, wind-tunnel exposures at a nominal peak temperature of 1560 K, no growth of small defects was observed in up to 10 simulated reentry cycles. After the first two or three cycles, a buff-colored oxide resulting from oxidation of the coating covered the specimens so that small defects were no longer visible. Figure 10 shows a group of six specimens of coated FS85 after five wind-tunnel exposure cycles. Each contains a small, 0.1-mm coating defect in the center, but these are not visible because of coating oxide overgrowth. The larger, 0.1-cm defects (in other specimens) were readily visible, but grew slowly, so that after ten wind-tunnel-simulated reentry cycles, they had grown to only about 0.13 cm in diameter. Under these lower temperature conditions, actual loss of metal to oxidation is minor in relation to property degradation resulting from oxygen

contamination. Figure 11 shows, in metallographic cross-section, the negligible growth of a small defect after 100 furnace exposure cycles, and also the substantial spread of contamination in the columbium alloy substrate. (The coating spalling and cracking occurred when the specimen was manhandled after exposure.)

Mechanical Property Effects

Numerous tensile, creep, fatigue, and bend tests were conducted on the coated-plus-defected columbium alloy specimens before and after both arc-heated wind-tunnel and static (furnace) exposures at temperatures of not greater than 1590 K. The intent was to establish differences in property degradation attributable to exposure mode. Although all materials experienced some degradation due to the "worst-case" exposures, there was no difference in the amount of degradation experienced under dynamic versus static exposure conditions.

In brief summary, contamination associated with the small, nongrowing defects had only relatively minor effects on mechanical properties. No gross degradation in useful structural properties was observed.

At large defect sites, degradation assumed more macroscopic proportions. It was found that the Cb752 and C129Y substrates were much more severely degraded than was the FS85 substrate. For example, the fracture strength of contaminated material surrounding large defects was noticeably decreased following as few as 3 or 4 exposure cycles for Cb752 and especially C129Y, but the associated strength in FS85 remained stable throughout at least 10 exposure cycles as shown in Figure 12. Some specimens of C129Y and Cb752 failed by catastrophic and total brittle fracture in tensile tests. Specimens of FS85 always failed "safely" by ductile shear. In high-cycle fatigue tests, the life of coated Cb752 at a stress level of about 275 MN/m^2 was reduced from about one million cycles to essentially zero cycles by the presence of contamination surrounding large defects following five exposure cycles. In contrast, no degradation was observed in comparison tests of coated, defected, and exposed FS85.

CONCLUSIONS

The following conclusions are valid in the context of the considered use of coated columbium alloys for which this evaluation was designed, namely, space shuttle orbiter thermal protection system hardware:

- Under conditions of hypersonic flow, rapid growth of defects in some coated columbium alloys occurs at temperatures above 1620 K. This is lower by about 80 K than the temperature required for similar growth rates under static oxidation conditions. In general, columbium

alloys should not be used in hypersonic, oxidizing environments at temperatures greater than 1620 K.

- At temperatures less than 1620 K, mechanical property stability of coated columbium alloys is not influenced by environmental flow dynamics at reasonably high levels of oxidation potential.

- For potential service at 1620 K, small coating defects are well tolerated by columbium alloys. Large coating defects can result in serious degradation in mechanical properties. Of the alloys studied, Cb752 and C129Y were seriously degraded; FS85 was not.

- Apparent degradation in coating/substrate emittance of coated columbium alloys occurs under multicycle hypersonic shear exposure conditions. Similar changes in surface emittance are not observed in furnace exposure conditions.

REFERENCES

(1) Pollack, F. G. and Hickel, R. O., "Surface Temperature Mapping with Infrared Photographic Pyrometry for Turbine Cooling Investigations", NASA TND-5179, January, 1969.

(2) Bartlett, E. S., et al, "Degradation and Reuse of Radiative-Thermal-Protection-System Materials for the Space Shuttle", Final Report to NASA-Marshall Space Flight Center, Contract No. NAS 8-26205, August 26, 1972.

(3) Kistler, C. W., et al, "Evaluation of Nonmetallic Thermal Protection Materials for the Manned Space Shuttle", Volume V, Final Report to NASA-Manned Spacecraft Center, Contract NAS 9-10853, June 1, 1972.

(4) Lordi, J. A., et al, "Computer Program for the Numerical Solution of Nonequilibrium Expansions of Reacting Gas Mixtures", NASA CR-472 (1965), 120 pp.

(5) Cohen, C. B. and Reshotko, E., "The Compressible Laminar Boundary Layer with Heat Transfer and Arbitrary Pressure Gradient", NACA Report 1294 (1956), 16 pp.

(6) Harney, D. J. and Petrie, S. L., "Hypersonic Surface Pressure and Heat Transfer on Slender Bodies in Variable Composition and Nonequilibrium Atmospheres", AFFDL-TR-70-31 (April, 1970), 42 pp.

TABLE 1. ENVIRONMENTAL CONDITIONS FOR COLUMBIUM ALLOY EXPOSURES

Specimen Type	Surface Temperature, K	Free Stream Mach Number	Heater Reservoir Pressure, kN/m^2	Gas Total Enthalpy, MJ/kg	Average Surface Pressure, kN/m^2	Average Surface Shear Stress, N/m^2	
						Front Specimens	Rear Specimens
Coated columbium alloy	1561	4.5	102-132	10.9-13.4	1.7	82	106
Coated columbium alloy	1644	4.5	112-132	13.4-16.0	2.1	87	116

TABLE 2. COMPARISON OF MEASURED AND CALCULATED HEAT TRANSFER RATES FOR COATED COLUMBIUM ALLOY WIND TUNNEL EXPOSURES

Nominal Specimen Surface Temperature K	Calorimeter Location Distance from Specimen Leading Edge, cm	Measured Cold Wall Heat Flux W/m^2	Calculated Cold Wall Heat Flux, W/m^2 (a)	Calculated Cold Wall Heat Flux, W/m^2 (b)	Measured Cold Wall Heat Flux Corrected to Nominal Specimen Temperature W/m^2
		Front Specimen			
1644	2.29	60.4×10^4	61.7×10^4	63.9×10^4	43.0×10^4
	5.33	51.3×10^4	51.0×10^4	52.1×10^4	37.4×10^4
		Rear Specimen			
	2.29	51.2×10^4	52.9×10^4	64.7×10^4	37.4×10^4
	5.33	44.5×10^4	42.6×10^4	52.5×10^4	31.7×10^4
		Front Specimen			
1561	2.29	38.2×10^4	37.4×10^4	42.4×10^4	27.5×10^4
	5.33	33.5×10^4	33.2×10^4	37.6×10^4	24.0×10^4
		Rear Specimen			
	2.29	38.0×10^4	31.5×10^4	42.8×10^4	27.3×10^4
	5.33	34.6×10^4	28.0×10^4	37.8×10^4	25.0×10^4

(a) Method from Harney, D. J. and Petrie, S. L., "Hypersonic Surface Pressure and Heat Transfer on Slender Bodies in Variable Composition and Nonequilibrium Atmospheres", AFFDL-TR-31 (April, 1970), 42 pp.

(b) Method from Hankey, W. L., Jr., et al, "Design Procedures for Computing Aerodynamic Heating at Hypersonic Speeds", WADC-TR-59-610 (June, 1960), 157 pp.

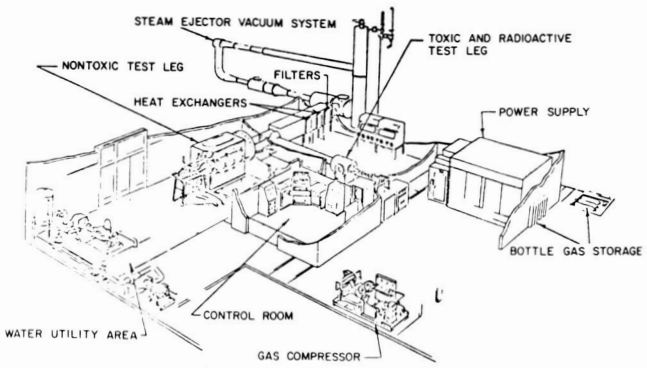

FIGURE 1. SCHEMATIC OF AEROTHERMAL RESEARCH FACILITY

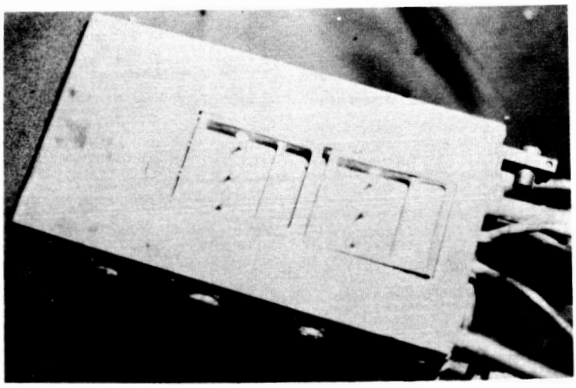

FIGURE 2. PHOTOGRAPH OF SPECIMEN MODEL HOLDER

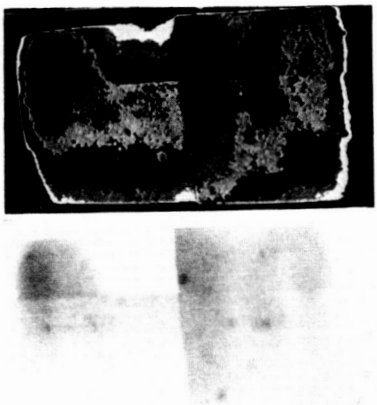

FIGURE 3. BLACK AND WHITE (BOTTOM) AND COLOR ENHANCED (TOP) INFRARED PHOTOGRAPH

(AIR FLOW FROM LEFT TO RIGHT)

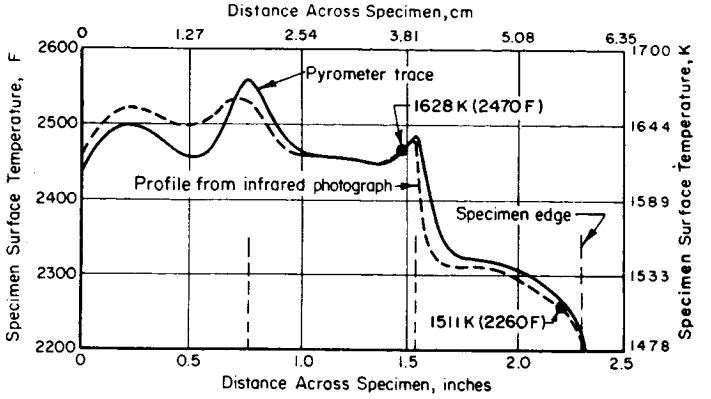

FIGURE 4. COMPARISON OF PYROMETER TEMPERATURE AND INFRARED PHOTOGRAPHIC TEMPERATURE DISTRIBUTION DATA

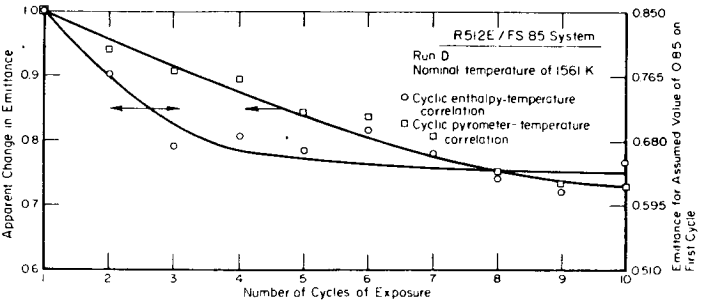

FIGURE 5. VARIATION IN EMITTANCE OF COATED COLUMBIUM ALLOY DURING MULTICYCLE WIND TUNNEL EXPOSURE.

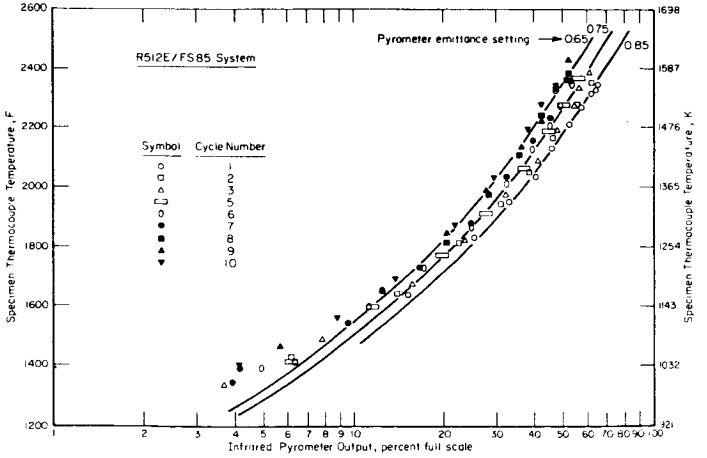

FIGURE 6. CHANGE IN EMITTANCE OF COATED COLUMBIUM DURING COOL-DOWN PORTION OF MULTICYCLE WIND TUNNEL EXPOSURE

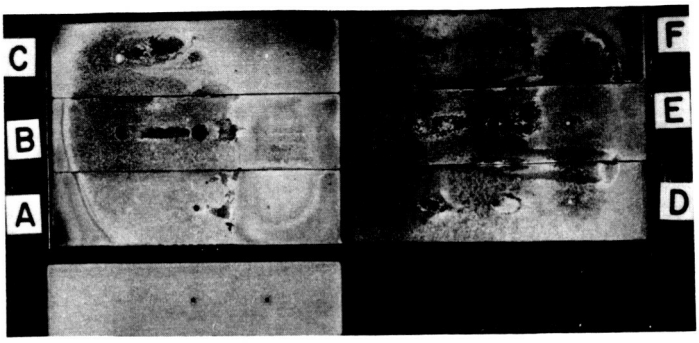

FIGURE 7. SPECIMENS FOLLOWING ONE REENTRY CYCLE AT 1644 K.

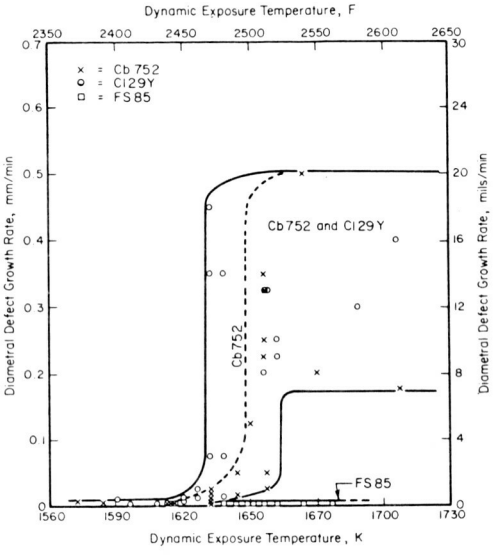

FIGURE 8. DEPENDENCE OF DEFECT GROWTH RATES ON TEMPERATURE.

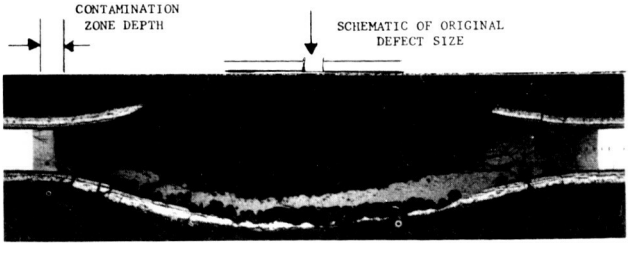

FIGURE 9. DEFECT GROWTH; ONE WIND TUNNEL EXPOSURE CYCLE AT 1644 K. (25X)

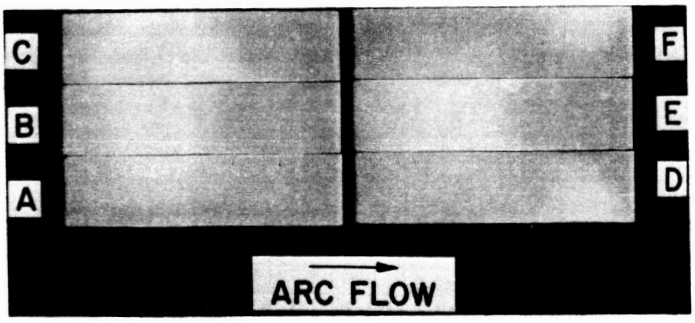

FIGURE 10. SPECIMENS FOLLOWING FIVE WIND TUNNEL CYCLES AT 1560 K.

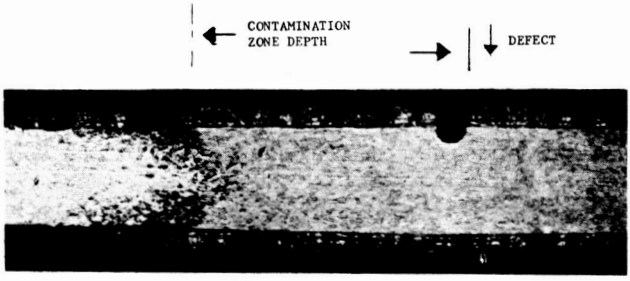

FIGURE 11. SMALL STABLE DEFECT FOLLOWING 100 FURNACE EXPOSURE CYCLES. (42X)

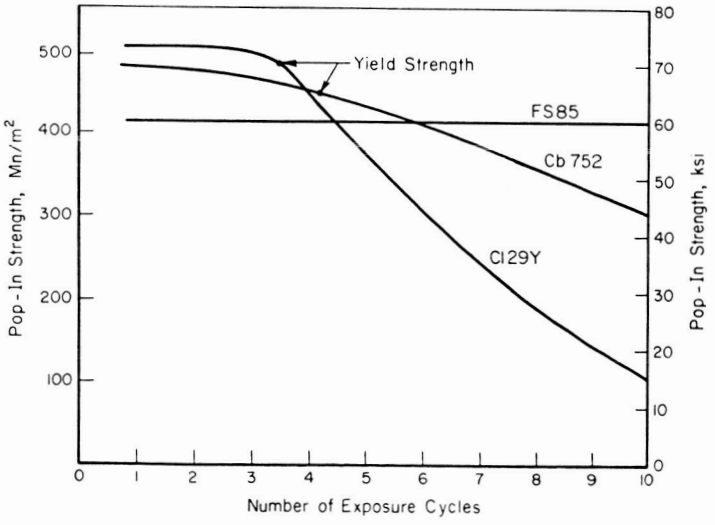

FIGURE 12. DEGRADATION IN FRACTURE STRENGTH OF CONTAMINATED COLUMBIUM ALLOYS ASSOCIATED WITH LARGE COATING DEFECTS.